Geophys. J. Int. (1996) **125**, 584–598

Two-dimensional multivalued traveltime and amplitude maps by uniform sampling of a ray field

G. Lambaré,[1] P. S. Lucio[1] and A. Hanyga[2]

[1] *École des Mines de Paris, Centre de Recherche en Géophysique, 35 rue Saint Honoré, 77 305 Fontainebleau, France*
[2] *Institute for Solid Earth Physics, University of Bergen, Allegaten* 41, 5007 *Bergen, Norway*

Accepted 1996 January 8. Received 1995 December 18; in original form 1994 July 28

SUMMARY

An algorithm for computing multivalued maps for traveltime, amplitude or any other ray-related variable is presented. It is based on a wavefront construction method, where the ray field is decomposed into elementary cells defined by adjacent rays and wavefronts. A sampling criterion for ray density in the phase space is suggested. It is demonstrated that this new criterion ensures uniform ray density over the entire ray field including caustics. The method is applied to complex models.

Key words: Green's functions, numerical techniques, ray theory, ray tracing, traveltime, wave propagation.

1 INTRODUCTION

The current interest in 3-D imaging has increased the importance of asymptotic methods of wavefield computation based on ray tracing. Migration and inversion requires repeated evaluation of the wavefield in the scattering region from several sources. Asymptotic methods offer a reasonable compromise between accuracy and computational efficiency (Hanyga & Helle 1995). In 3-D inversion/migration, the task is formidable and asymptotic methods become unavoidable. The efficient numerical calculation of traveltimes and amplitudes is a major challenge in imaging by asymptotic methods. A significant breakthrough was achieved through the finite-difference (FD) calculation of the first-arrival traveltime (Vidale 1988; Podvin & Lecomte 1991). However, FD computation of traveltimes leads to poor imaging in complex media (Geoltrain & Brac 1991), owing to unreliable amplitude information. The simultaneous computation of traveltimes and amplitudes is possible by dynamic ray tracing of a densely and uniformly sampled ray field, and evaluation of traveltimes and asymptotic ray theory (ART) amplitudes at a given point by interpolation (Lambaré *et al.* 1992; Vinje *et al.* 1993a,b; Sun 1992; Forgues *et al.* 1994).

The ray density has to be controlled in order to ensure accuracy as well as computational efficiency of the algorithm. Ray density can be checked at some selected places, such as at a sequence of flat horizons (Lambaré *et al.* 1992) or wavefronts (Vinje *et al.* 1993a,b; Sun 1992). The latter approach is followed in this paper. In order to keep the ray density above a minimum level it is necessary to insert additional rays as the ray field spreads out from the source. An additional ray is generated by interpolation of initial data and subsequent tracing of the ray.

Two criteria for ray density have previously been suggested, namely the metric distance between adjacent rays (Lambaré *et al.* 1992; Vinje *et al.* 1993a,b) and their angular distance (Sun 1992). Instead of directly addressing the problem of the precision of the ray-field sampling, these criteria attempt to control ray density by a loosely related input parameter. As the control parameter is not directly related to the complexity of the ray field, each particular computation requires at least some visualization of the ray field in order to check the quality of the result. The shortcomings of the above-mentioned algorithms are particularly apparent in caustic regions.

We propose a method for calculating multivalued traveltime and amplitude maps in 2-D smooth heterogeneous velocity fields. Our approach is based on the wavefront construction method initially proposed by Vinje, Iversen & Gjøystdal (1992) and on the Hamiltonian formulation of ray tracing.

The Hamiltonian formulation (Goldstein 1980) is a very convenient tool in seismic ray theory (see Burridge 1976; Hanyga, Lenartowicz & Pajchel 1985; Chapman 1985; Červený 1989; Virieux & Farra 1991). In the Hamiltonian approach, rays in the configuration space $(\mathbf{x})$ are replaced by bicharacteristic curves in the phase space $(\mathbf{x}, \mathbf{p})$, where $\mathbf{p}$ denotes the slowness vector. These trajectories, defined as the integral curves of the Hamiltonian equations for a fixed source, do not intersect at caustics. In the space $(\mathbf{x}, \mathbf{p})$, the bicharacteristics span a regular Lagrangian submanifold Λ (Maslov 1972; Hanyga 1984; Hanyga *et al.* 1985). The submanifold Λ can be parametrized by two globally defined coordinates, namely the traveltime σ and the take-off angle θ. The ray-related variables are smooth functions of the coordinates (σ, θ) and consequently it is possible to interpolate them on Λ. The tangent planes to Λ can be determined at every point by paraxial ray tracing.

We propose to sample the ray field along rays by a method

of wavefront construction. The ray field is paved by elementary quadrangular cells defined by adjacent rays and wavefronts. The cell sizes are checked to ensure a uniform precision of the interpolation of the submanifold Λ along the sampled wavefronts. First-order interpolation is used and an upper limit on the local misfit of the submanifold Λ with its tangent plane is used to constrain the ray density. Each elementary cell is projected and interpolated over a regular grid in (x, z). We present applications of our algorithm to some complex models.

2 HAMILTONIAN FORMULATION OF RAY THEORY

The Hamiltonian for an isotropic medium can be written in the form

$$H(\mathbf{x}, \mathbf{p}) = \frac{1}{2}\left(\frac{\mathbf{p}^2}{u^2(\mathbf{x})} - 1\right), \tag{1}$$

where $\mathbf{x}$ is the ray position, $\mathbf{p}$ the slowness vector associated with the ray, σ the internal coordinate on every ray (σ has the dimension of time) and $u(\mathbf{x})$ the slowness. Bicharacteristics $(\mathbf{x}, \mathbf{p})(\sigma)$ in the phase space satisfy a system of canonical or ray differential equations:

$$\begin{cases} \dfrac{\partial \mathbf{x}}{\partial \sigma} = \nabla_p H = \mathbf{p}/u^2(\mathbf{x}), \\ \dfrac{\partial \mathbf{p}}{\partial \sigma} = -\nabla_x H = \dfrac{1}{2}\dfrac{\mathbf{p}^2}{u^4(\mathbf{x})}\nabla u^2(\mathbf{x}). \end{cases} \tag{2}$$

The eikonal equation is satisfied if the Hamiltonian vanishes all along the bicharacteristics: $H(\mathbf{x}, \mathbf{p}) = 0$. Since the Hamiltonian does not depend on σ it is constant along any bicharacteristic and it is sufficient to ensure that it vanishes at the source point.

Traveltime is given by the integration of slowness along the trajectory of the rays:

$$T(\mathbf{x}(\sigma)) = T(\mathbf{x}(\sigma_0)) + \int_{\sigma_0}^{\sigma} \mathbf{p} \cdot \frac{\partial \mathbf{x}}{\partial \sigma}\, d\sigma = T(\mathbf{x}(\sigma_0)) + \sigma - \sigma_0, \tag{3}$$

where $\cdot$ denotes the scalar product, whence σ coincides with traveltime, up to an additive constant.

3 PARAXIAL RAY EQUATIONS

Linear interpolation of ray-field variables as well as amplitude computation is based on paraxial ray tracing (Chapman 1985; Farra & Madariaga 1987). A perturbation of the bicharacteristic $(\delta\mathbf{x}, \delta\mathbf{p})$ around a central bicharacteristic (Fig. 1) satisfies, in the first-order approximation, a linear system of ordinary

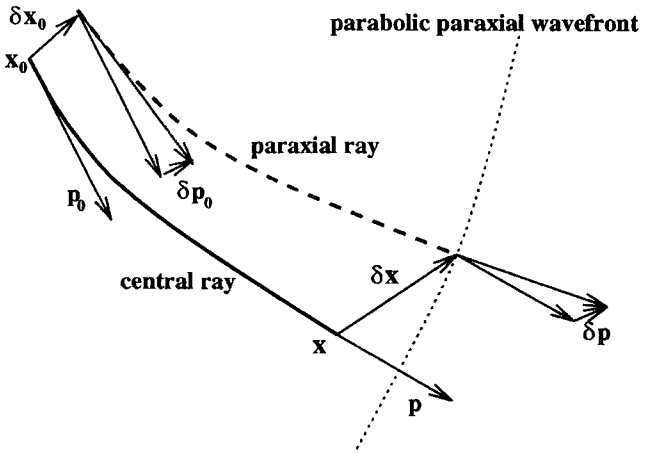

Figure 1. Paraxial approximation around a central ray. The parabolic paraxial wavefront is shown.

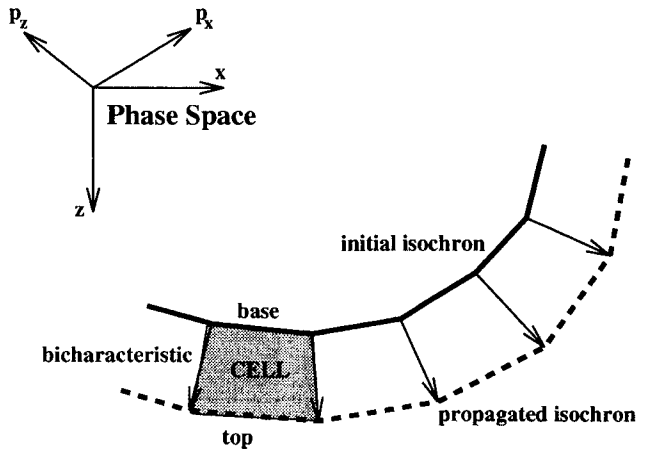

Figure 2. The paving of the Lagrangian manifold. The Lagrangian manifold is paved with quadrangular cells defined in terms of bicharacteristics and isochrons.

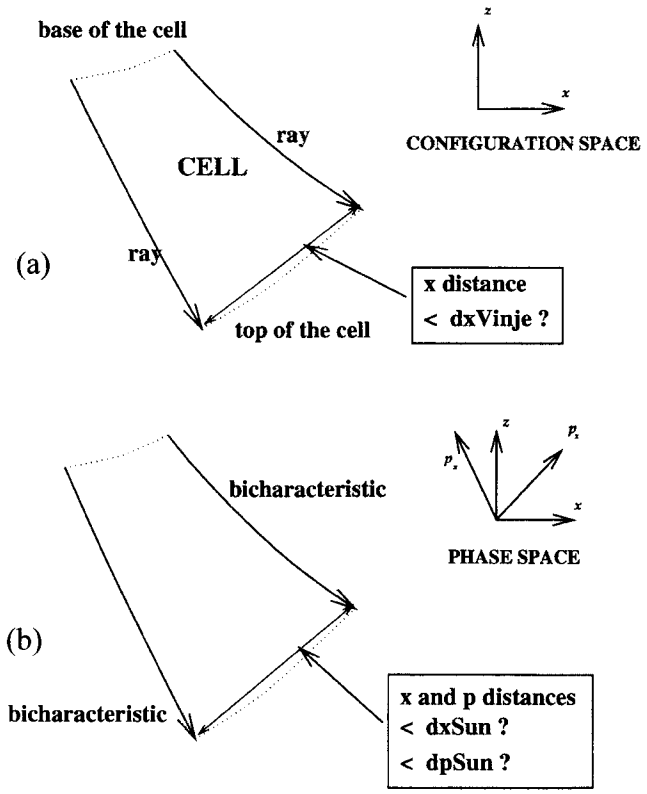

Figure 3. Vinje's and Sun's criteria for checking the size of the cells. (a) Vinje's criterion, where the $\mathbf{x}$ distance of the top of the cell must not exceed the value dx_{Vinje}. (b) Sun's criterion, where the $\mathbf{x}$ and $\mathbf{p}$ distances of the top of the cell must not exceed the values dx_{Sun} and dp_{Sun}.

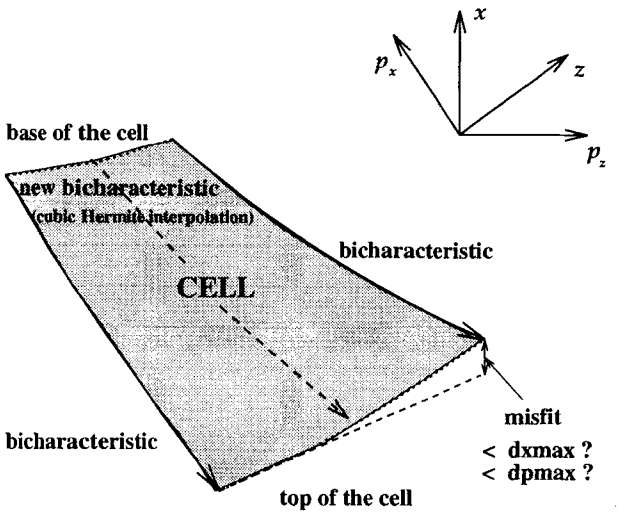

Figure 4. Our new criterion for checking the size of the cells. The misfit between the tangent plane (defined by the paraxial approximation) and the exact manifold must not exceed a given value in distance and slowness. A new bicharacteristic is interpolated at the base of the cell if the misfit exceeds $(dx_{\max}, dp_{\max})$.

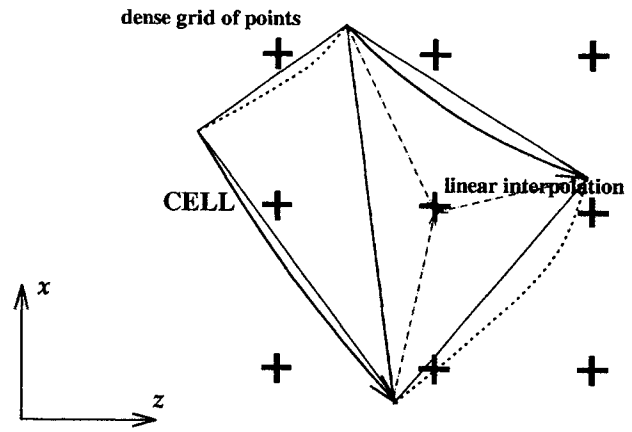

Figure 5. Linear interpolation in the configuration space. Each cell on the Lagrangian manifold is projected on the configuration space. It is subdivided into two triangles. A dense regular grid is defined in each triangle. Values of the ray-field variables at the grid points are determined by linear interpolation from the values at the vertices of triangles.

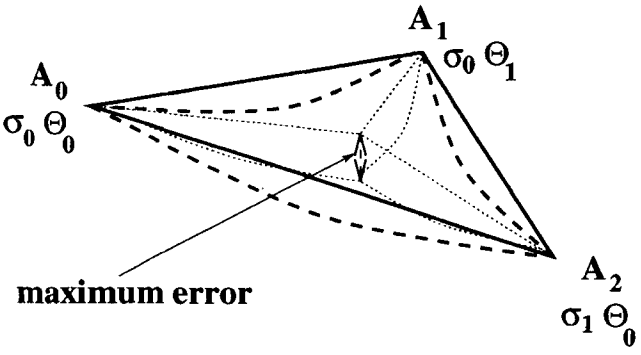

Figure 6. Accuracy of the linear interpolation. Paraxial ray theory provides an estimation for the error associated with our linear interpolation.

differential equations:

$$\begin{cases} \dfrac{\partial \delta \mathbf{x}}{\partial \sigma} = \nabla_x \nabla_p H \cdot \delta \mathbf{x} + \nabla_p \nabla_p H \cdot \delta \mathbf{p} \\ \qquad = -\dfrac{\mathbf{p}}{u^4(\mathbf{x})}(\nabla u^2(\mathbf{x}) \cdot \delta \mathbf{x}) + \dfrac{1}{u^2(\mathbf{x})}\delta \mathbf{p}, \\ \dfrac{\partial \delta \mathbf{p}}{\partial \sigma} = -\nabla_x \nabla_x H \cdot \delta \mathbf{x} - \nabla_p \nabla_x H \cdot \delta \mathbf{p} \\ \qquad = \dfrac{1}{2}\dfrac{\mathbf{p}^2}{u^4(\mathbf{x})}\nabla\nabla u^2(\mathbf{x})\delta \mathbf{x} - \dfrac{\mathbf{p}^2}{u^6(\mathbf{x})}\nabla u^2(\mathbf{x})(\nabla u^2(\mathbf{x}) \cdot \delta \mathbf{x}) \\ \qquad + \dfrac{1}{u^4(\mathbf{x})}\nabla u^2(\mathbf{x})(\mathbf{p} \cdot \delta \mathbf{p}). \end{cases} \tag{4}$$

The eikonal equation implies that the first-order perturbation δH of the Hamiltonian vanishes along the perturbed ray trajectory:

$$\delta H(\mathbf{x}, \mathbf{p}) = \nabla_x H \cdot \delta \mathbf{x} + \nabla_p H \cdot \delta \mathbf{p} = -\frac{1}{2}\frac{\mathbf{p}^2}{u^4(\mathbf{x})}\nabla u^2(\mathbf{x}) \cdot \delta \mathbf{x} + \frac{1}{u^2(\mathbf{x})}\mathbf{p} \cdot \delta \mathbf{p} = 0. \tag{5}$$

The linear differential system of equations (4) can be solved by the propagator matrix method (Aki & Richards 1980). The solution is given in terms of a propagator matrix $\mathbf{P}$, such that

$$\begin{pmatrix} \delta \mathbf{x} \\ \delta \mathbf{p} \end{pmatrix}(\sigma) = \mathbf{P}(\sigma, \sigma_0)\begin{pmatrix} \delta \mathbf{x} \\ \delta \mathbf{p} \end{pmatrix}(\sigma_0). \tag{6}$$

This matrix is defined as the 4×4 Jacobian matrix

$$\mathbf{P}(\sigma, \sigma_0) = \frac{\partial(\mathbf{x}, \mathbf{p})}{\partial(\mathbf{x}_0, \mathbf{p}_0)} = \begin{pmatrix} \mathbf{Q}_1 & \mathbf{Q}_2 \\ \mathbf{P}_1 & \mathbf{P}_2 \end{pmatrix}, \tag{7}$$

where $\mathbf{Q}_1$, $\mathbf{Q}_2$, $\mathbf{P}_1$ and $\mathbf{P}_2$ are 2×2 matrices (Farra & Madariaga 1987). It satisfies the linear system of ordinary differential equations

$$\frac{\partial \mathbf{P}}{\partial \sigma} = \begin{pmatrix} \nabla_x \nabla_p H & \nabla_p \nabla_p H \\ -\nabla_x \nabla_x H & -\nabla_p \nabla_x H \end{pmatrix}\mathbf{P}, \tag{8}$$

where $\mathbf{P}(\sigma_0, \sigma_0) = \mathbf{I}$ (initial condition) and the determinant of $\mathbf{P}$ is equal to 1 (Liouville's theorem, Goldstein 1980).

4 RAY FIELD AND LAGRANGIAN MANIFOLD

A 2-D ray field is naturally parametrized by any coordinate θ specifying the initial direction of the rays (the take-off angle in the case of a point-source radiation) and an internal coordinate σ of the rays.

In the phase space $(\mathbf{x}, \mathbf{p})$ the bicharacteristics parametrized by (θ, σ) span a submanifold Λ (Pham 1992). The manifold Λ is locally represented by graphs of smooth functions such as $\nabla T(\mathbf{x})$, and consequently is Lagrangian and regular (Guillemin & Sternberg 1977; Weinstein 1979). Λ can in general fold over the configuration space $(\mathbf{x})$. Caustics of the ray field are images of the folds of Λ under the projection mapping $(\mathbf{x}, \mathbf{p}) \rightarrow (\mathbf{x})$ (Hanyga *et al.* 1985). Consequently, at the caustics the projection of Λ: $(\theta, \sigma) \rightarrow (x, z)$ is singular (non-invertible), and many functions associated with the ray field cannot be expressed as smooth functions of the configuration space coordinates (x, z).

The tangent planes of Λ in the phase space are given by the

partial derivatives of the coordinates $(\mathbf{x}, \mathbf{p})$ with respect to θ and σ. They can be expressed in terms of paraxial quantities $\partial(\mathbf{x}, \mathbf{p})/\partial\sigma$ and $\partial(\mathbf{x}, \mathbf{p})/\partial\theta$, and, consequently, in terms of their initial values and the propagator matrices:

$$\begin{cases} \dfrac{\partial}{\partial\sigma}\begin{pmatrix}\mathbf{x}\\ \mathbf{p}\end{pmatrix}(\theta, \sigma) = \mathbf{P}(\sigma, \sigma_0)\dfrac{\partial}{\partial\sigma}\begin{pmatrix}\mathbf{x}\\ \mathbf{p}\end{pmatrix}(\theta, \sigma_0), \\ \dfrac{\partial}{\partial\theta}\begin{pmatrix}\mathbf{x}\\ \mathbf{p}\end{pmatrix}(\theta, \sigma) = \mathbf{P}(\sigma, \sigma_0)\dfrac{\partial}{\partial\theta}\begin{pmatrix}\mathbf{x}\\ \mathbf{p}\end{pmatrix}(\theta, \sigma_0), \end{cases} \tag{9}$$

where the partial derivatives with respect to σ are given by eq. (2).

In view of Liouville's theorem, regularity of Λ is ensured by the condition that the derivatives of $(\mathbf{x}, \mathbf{p})$ with respect to θ and σ are independent at any fixed value of σ_0, for example at the source.

Using eq. (9) it is possible to determine a beam of paraxial rays around a central ray. In order to describe the variation of rays in the beam we introduce the vector

$$\mathbf{J}(\sigma, \sigma_0) = \frac{\partial(\mathbf{x}, \mathbf{p})}{\partial\theta}(\sigma) = \mathbf{P}(\sigma, \sigma_0)\mathbf{J}(\sigma_0, \sigma_0), \tag{10}$$

where for a point source

$$\mathbf{J}(\sigma_0, \sigma_0) = \begin{pmatrix} 0 \\ 0 \\ p_{z0} \\ -p_{x0} \end{pmatrix}. \tag{11}$$

In the zero-order approximation of the ray theory, the amplitude A is given in terms of the geometrical spreading

$$\mathscr{J} = u^2(\mathbf{x})\left|\det\left[\frac{\partial(x, z)}{\partial(\sigma, \theta)}\right]\right|$$

by the equation

$$A(\sigma) = A(\sigma_0)\sqrt{\frac{\mathscr{J}(\sigma_0)}{\mathscr{J}(\sigma)}}. \tag{12}$$

We now describe a method to estimate the values of the parameters $(\mathbf{x}, \mathbf{p})$ and the traveltime $T(\mathbf{x})$ in the vicinity of a central ray for a given ray field. Suppose we know the values of the vector $\mathbf{J}$ and of the traveltime T_1 at the point $A_1 = (\mathbf{x}_1, \mathbf{p}_1) \in \Lambda$. We want to estimate the values of the slowness vector $\mathbf{p}_2$ and of the traveltime T_2 at a point $A_2 \in \Lambda$

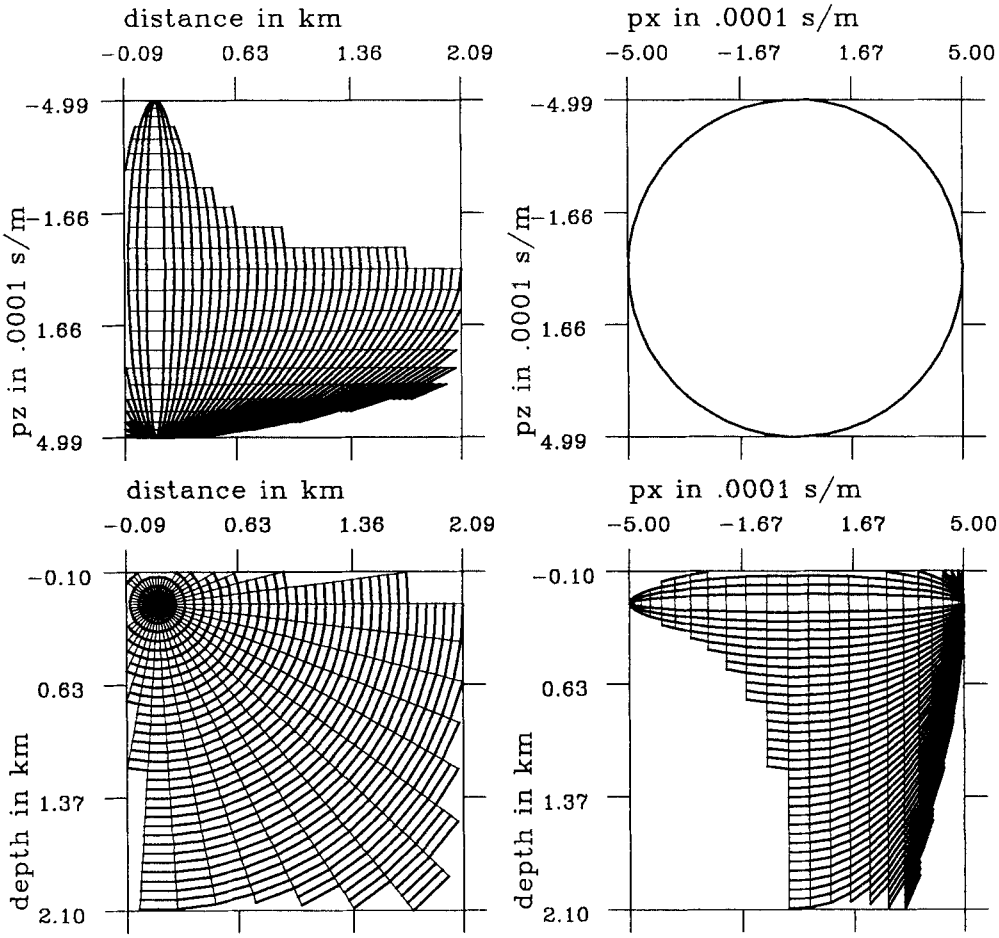

Figure 7. The Lagrangian manifold Λ for a constant-velocity field ($v = 2000\ \mathrm{m\ s^{-1}}$). The paving in the cells of Λ is shown for various 2-D projections of the phase space $[(x, z), (x, p_x), (p_x, z), (p_x, p_z)]$. The source point is at $x = 110$ m, $z = 110$ m. The traveltime step is 0.03 s, and the ray-density criterion is $dx_{\max} = 10$ m and $dp_{\max} = 10 \times 10^{-6}\ \mathrm{s\ m^{-1}}$. In the plane (x, z) the rays are straight lines and the wavefronts are circles.

corresponding to the point $\mathbf{x}_2$ in the vicinity of A_1. In the vicinity of A_1, we have the following relation between the perturbed parameters $(\delta\mathbf{x}, \delta\mathbf{p})$ and the perturbation $(\delta\sigma, \delta\theta)$:

$$\begin{pmatrix}\delta\mathbf{x}\\ \delta\mathbf{p}\end{pmatrix} = \frac{\partial}{\partial\sigma}\begin{pmatrix}\mathbf{x}\\ \mathbf{p}\end{pmatrix}\delta\sigma + \frac{\partial}{\partial\theta}\begin{pmatrix}\mathbf{x}\\ \mathbf{p}\end{pmatrix}d\theta, \tag{13}$$

where the partial derivatives are estimated at A_1. We estimate $\delta\sigma$ and $\delta\theta$ from the linear system consisting of eq. (13) and the definition of $\delta\mathbf{x}$: $\delta\mathbf{x} = \mathbf{x}_2 - \mathbf{x}_1$. We then obtain $\delta\mathbf{p}$ to the first order from eq. (13) and the traveltime to the second order from the relation

$$T_2 = T_1 + \mathbf{p}_1 \cdot \delta\mathbf{x} + \frac{1}{2}\delta\mathbf{p} \cdot \delta\mathbf{x}. \tag{14}$$

5 UNIFORM SAMPLING OF THE LAGRANGIAN MANIFOLD Λ

It remains to find a criterion for sampling the Lagrangian manifold Λ in the phase space (x, z, p_x, p_z). Drawing on the wavefront construction method proposed by Vinje *et al.* (1992, 1993a) and Sun (1992), we divide the Lagrangian manifold Λ into curvilinear quadrilateral cells. This approach has the advantage of an easy numerical implementation and of a possible extension to three dimensions (Vinje *et al.* 1993b; Lucio, Lambaré & Hanyga 1995). A cell is defined as the section of a ray tube bounded by two isochrons. It can be specified in terms of its four vertices (Fig. 2).

The cells are constructed proceeding along the rays from an initial set of cells. Some criterion must be chosen to control the cell size. An acceptable discretization of the coordinate σ can be based on a periodic sampling. Any other sampling, for example a constant step in z, could be chosen, but a constant traveltime step has a more direct physical meaning.

The sampling of θ must take into account the local ray-field complexity. A recently proposed criterion by Vinje *et al.* (1993a, b) is based on the maximum distance between rays on successive wavefronts. Consider the top of a cell defined by the two points $A_1(\mathbf{x}_1, \mathbf{p}_1)$ and $A_2(\mathbf{x}_2, \mathbf{p}_2)$ and associated with the bicharacteristics θ_1 and θ_2. Vinje's criterion imposes (Fig. 3a)

$$|\mathbf{x}_2 - \mathbf{x}_1| < dx_{\text{Vinje}}. \tag{15}$$

This criterion has the advantage of being simple, but it does not guarantee uniform accuracy of interpolation. In particular, the ray density is drastically underestimated in the vicinity of caustics. As a result, Vinje *et al.* (1993a) have to ignore some parts of the wavefront adjacent to caustics.

In order to overcome this limitation, Sun (1992) introduced an angular distance in addition to the metric distance between

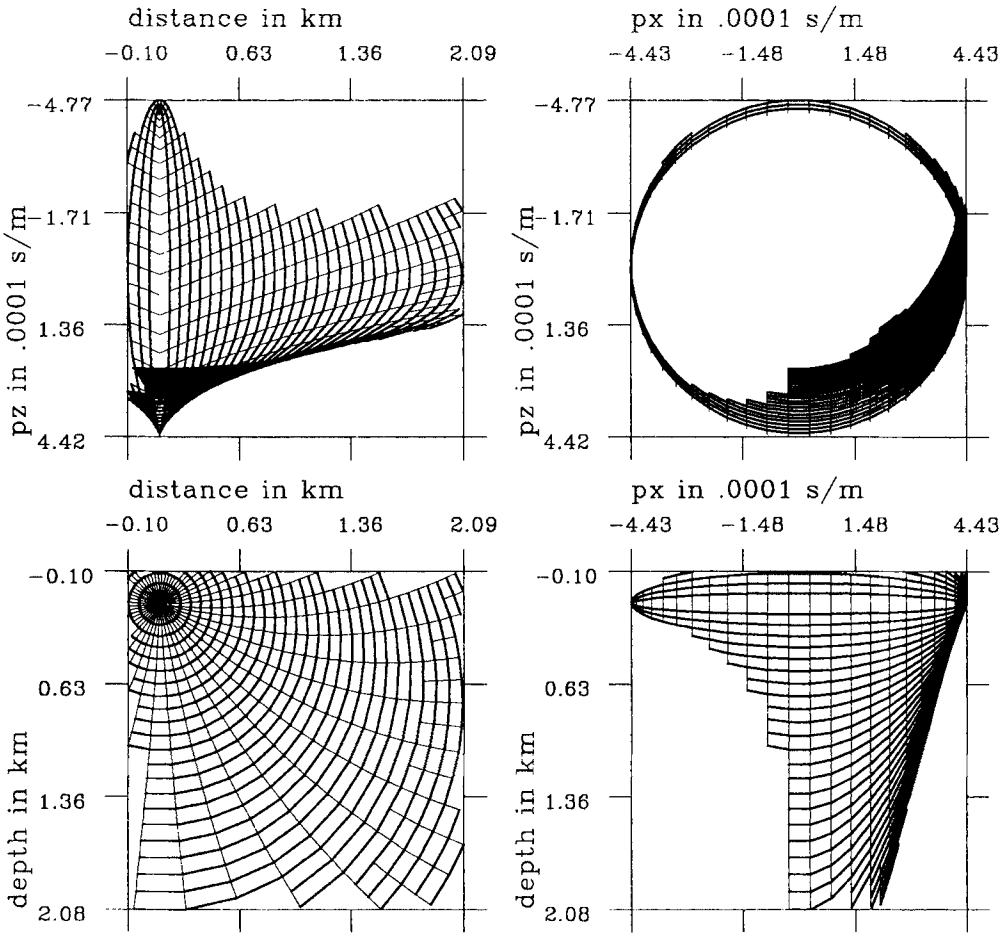

Figure 8. The Lagrangian manifold Λ for a constant-gradient velocity field. Velocity increases linearly with depth, from 2083 m s^{-1} at $z = 0$ m to 3833 m s^{-1} at $z = 2000$ m. The traveltime step is 0.03 s, and the ray-density criterion is $dx_{\max} = 10$ m and $dp_{\max} = 10 \times 10^{-6}$ s m^{-1}. In the (x, y) plane, the cells are defined by circular rays and wavefronts. Note the p-caustic at the bottom of the (x, p_z) projection.

rays. With respect to Vinje's criterion, this criterion has the advantage of taking into account in some way the distance between the rays in terms of slowness (even if it considers only the direction of the slowness). In this paper, a slightly altered version of Sun's criterion was used for tests, where the original angular distance was replaced by an equivalent test on slowness vectors (Fig. 3b):

$$\begin{cases} |\mathbf{x}_2 - \mathbf{x}_1| < dx_{\text{Sun}}, \\ |\mathbf{p}_2 - \mathbf{p}_1| < dp_{\text{Sun}}. \end{cases} \tag{16}$$

This choice was motivated by the simplicity of the expressions and by the fact that it retains the underlying philosphy. With respect to Vinje's criterion, Sun's one gives a better ray coverage in the vicinity of caustic cusps but no significant improvement in the case of simple caustics, where the slowness variation is often smaller. Numerical specification of Sun's criterion is still difficult, however, and in general ray density has to be overestimated to obtain an overall satisfying numerical precision.

A correct way to proceed should involve a criterion that ensures a uniform precision of the interpolation. Since we use a first-order interpolation, the local sampling density of the Lagrangian manifold Λ should be related to the curvature of Λ. A good criterion for estimating the curvature of the surface is the mismatch between a bicharacteristic and its paraxial approximation from an adjacent bicharacteristic. Two bicharacteristics R_1, R_2 are close enough if the estimate of R_2 obtained by linear approximation based on paraxial matrices computed for R_1 does not deviate too much from R_2 (Fig. 4).

Consider two points $(\mathbf{x}_1, \mathbf{p}_1)$ and $(\mathbf{x}_2, \mathbf{p}_2)$ on two different bicharacteristics and suppose that the corresponding values of σ, θ are σ_1, θ_1 and σ_2, θ_2. For a given perturbation of $\delta\theta = \theta_2 - \theta_1$ of the bicharacteristic θ_1 we can compute a paraxial estimate of the bicharacteristic θ_2. In the vicinity of point A_1 the coordinates $(\mathbf{x}, \mathbf{p})$ can be approximated in terms of $\delta\theta$ and $\delta\sigma$ by the linear equation

$$\begin{pmatrix} \delta\mathbf{x} \\ \delta\mathbf{p} \end{pmatrix} = \mathbf{J}_1 \delta\theta + \begin{pmatrix} \nabla_p H \\ -\nabla_x H \end{pmatrix}_1 \delta\sigma, \tag{17}$$

where $\mathbf{J}_1$ denotes the value of $\mathbf{J}$ at $(\mathbf{x}_1, \mathbf{p}_1)$. We compare a point A_2 on the isochron ($\delta\sigma = 0$) through A_1 with the linear approximation given by eq. (17). The above criterion amounts to an upper limit on the error in distance and slowness:

$$\begin{cases} |\delta\mathbf{x} + \mathbf{x}_1 - \mathbf{x}_2| \leq dx_{\max}, \\ |\delta\mathbf{p} + \mathbf{p}_1 - \mathbf{p}_2| \leq dp_{\max}. \end{cases} \tag{18}$$

As we will see later, this criterion is related to the curvature of the Lagrangian manifold Λ along the isochrons.

Following the idea of Sun (1992) and Vinje *et al.* (1993a,b), a new bicharacteristic is traced from the base of the cell when two end points of the bicharacteristics turn out to be too far apart at the top of the cell. The parameters of the new bicharacteristic are interpolated in the phase space at the base of the cell (Fig. 4). Cubic Hermite interpolation (Farin 1993) in θ is used for $\mathbf{x}, \mathbf{p}$ and traveltime. In order to ensure the embedding of the cells in the space $(\mathbf{x})$, the new interpolated point has to be on the base of the cell. An abscissa α is introduced such that $\mathbf{x}(\alpha) = \mathbf{x}_1 + (\mathbf{x}_2 - \mathbf{x}_1)\alpha$, and derivatives with respect to α of parameters are given by combinations of the paraxial parameters.

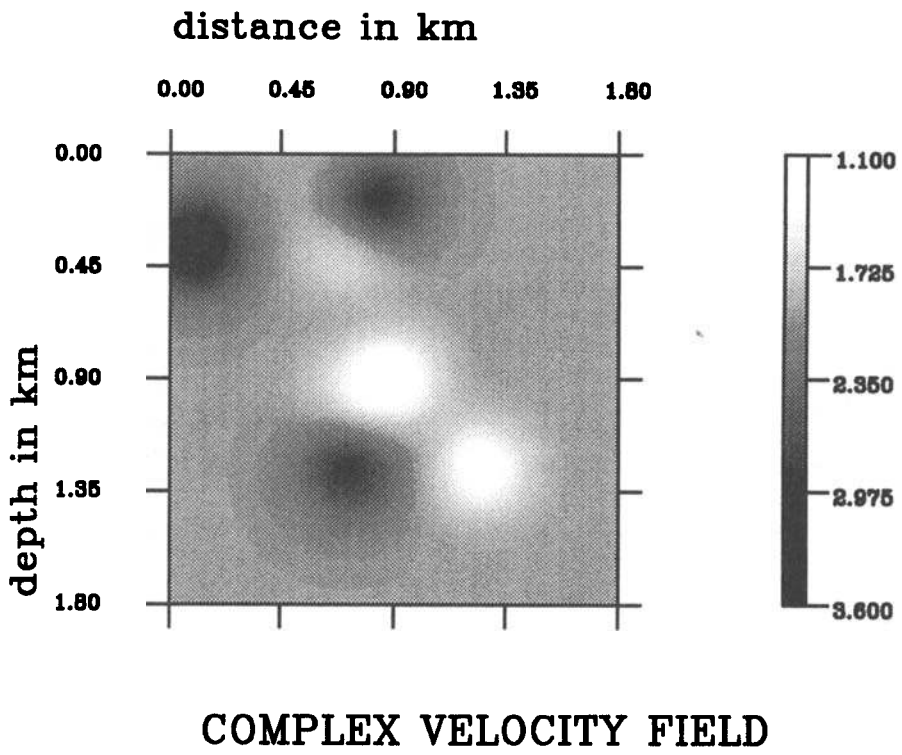

Figure 9. A complex velocity field. 25 × 25 knot points spaced by 100 m are used for the B-spline representation of the velocity field. The velocity ranges from 1093 m s^{-1} to 3800 m s^{-1}.

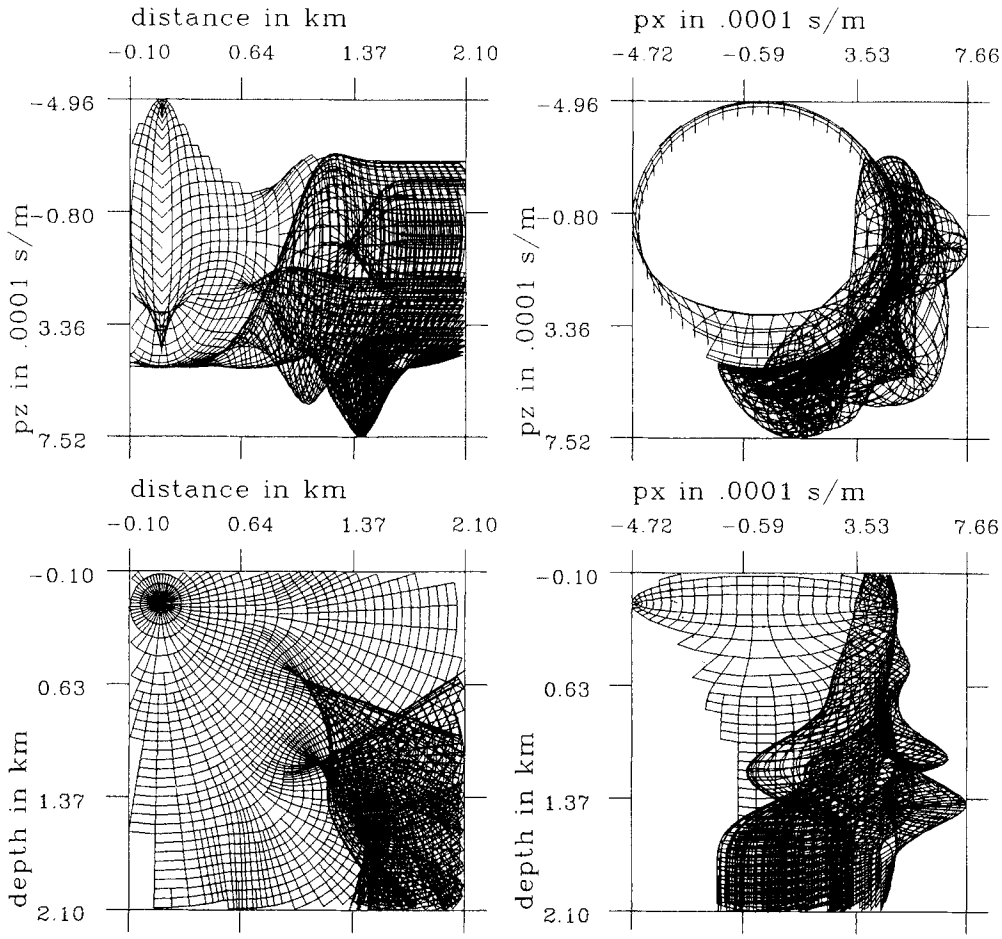

Figure 10. The Lagrangian manifold Λ in a complex velocity field. The criterion (18) has been applied. The source is at $x = 110$ m, $z = 110$ m. The traveltime step is 0.03 s, and the ray density is specified by criterion (18) with $dx_{\max} = 10$ m and $dp_{\max} = 10 \times 10^{-6}$ s m^{-1}. The ray field exhibits many caustics, and projections involve many overlapping cells. The density of rays in the configuration space is increased in the regions of strong curvature of the rays.

6 INTERPOLATION INSIDE THE CELLS

For interpolating the results obtained at cell vertices on a denser grid of points we use a robust first-order scheme. Each cell is divided into two triangles according to a criterion of the smallest misfit in position and slowness between the opposite edges of the cell. A dense grid is defined in each triangle. For each grid point, the values of $(\mathbf{p}, \theta, T, \mathbf{J})$ are evaluated by linear interpolation from the values at the vertices of the triangle (Fig. 5). The precision of linear interpolation on the ray field can be then estimated with the help of paraxial theory.

Suppose that on a given triangle $A_0(\theta_0, \sigma_0)$, $A_1(\theta_1, \sigma_0)$ and $A_2(\theta_0, \sigma_1)$, Λ is approximated by a quadratic expression:

$$\begin{cases} \mathbf{x}(\theta, \sigma) = \mathbf{x}_0 + \mathbf{a}_x \Delta\sigma + \mathbf{b}_x \Delta\theta + \mathbf{c}_x (\Delta\sigma)^2 + \mathbf{d}_x \Delta\sigma\Delta\theta + \mathbf{e}_x (\Delta\theta)^2, \\ \mathbf{p}(\theta, \sigma) = \mathbf{p}_0 + \mathbf{a}_p \Delta\sigma + \mathbf{b}_p \Delta\theta + \mathbf{c}_p (\Delta\sigma)^2 + \mathbf{d}_p \Delta\sigma\Delta\theta + \mathbf{e}_p (\Delta\theta)^2, \end{cases} \tag{19}$$

where $\Delta\sigma = \sigma - \sigma_0$ and $\Delta\theta = \theta - \theta_0$.

Linear interpolation of $\mathbf{x}, \mathbf{p}$ on the triangle yields the following (Fig. 6) estimates:

$$\begin{cases} \mathbf{x}_{\text{int}}(\theta, \sigma) = \mathbf{x}_0 + \dfrac{\mathbf{x}_2 - \mathbf{x}_0}{\sigma_1 - \sigma_0} \Delta\sigma + \dfrac{\mathbf{x}_1 - \mathbf{x}_0}{\theta_1 - \theta_0} \Delta\theta, \\ \mathbf{p}_{\text{int}}(\theta, r) = \mathbf{p}_0 + \dfrac{\mathbf{p}_2 - \mathbf{p}_0}{\sigma_1 - \sigma_0} \Delta\sigma + \dfrac{\mathbf{p}_1 - \mathbf{p}_0}{\theta_1 - \theta_0} \Delta\theta. \end{cases} \tag{20}$$

This result can be compared with the second-order approximation (19). An estimate of the maximum error of the approximation (20) is restricted by the inequalities

$$|\mathbf{x}_{\text{int}} - \mathbf{x}| < \frac{1}{8} \left| \frac{\partial^2 \mathbf{x}}{\partial r^2} \right| \Delta\sigma_1^2 + \frac{1}{8} \left| \frac{\partial^2 \mathbf{x}}{\partial \theta^2} \right| \Delta\theta_1^2 + \frac{1}{4} \left| \frac{\partial^2 \mathbf{x}}{\partial\theta\partial\sigma} \right| \Delta\sigma_1 \Delta\theta_1 \tag{21}$$

and

$$|\mathbf{p}_{\text{int}} - \mathbf{p}| < \frac{1}{8} \left| \frac{\partial^2 \mathbf{p}}{\partial \sigma^2} \right| \Delta\sigma_1^2 + \frac{1}{8} \left| \frac{\partial^2 \mathbf{p}}{\partial \theta^2} \right| \Delta\theta_1^2 + \frac{1}{4} \left| \frac{\partial^2 \mathbf{p}}{\partial\theta\partial\sigma} \right| \Delta\sigma_1 \Delta\theta_1 \tag{22}$$

($|\cdot|$ denotes here the vector norm, $\Delta\sigma_1 = |\sigma_1 - \sigma_0|$ and $\Delta\theta_1 = |\theta_1 - \theta_0|$). The partial derivatives with respect to σ are given by eqs (2) and (4). The first-order derivatives with respect

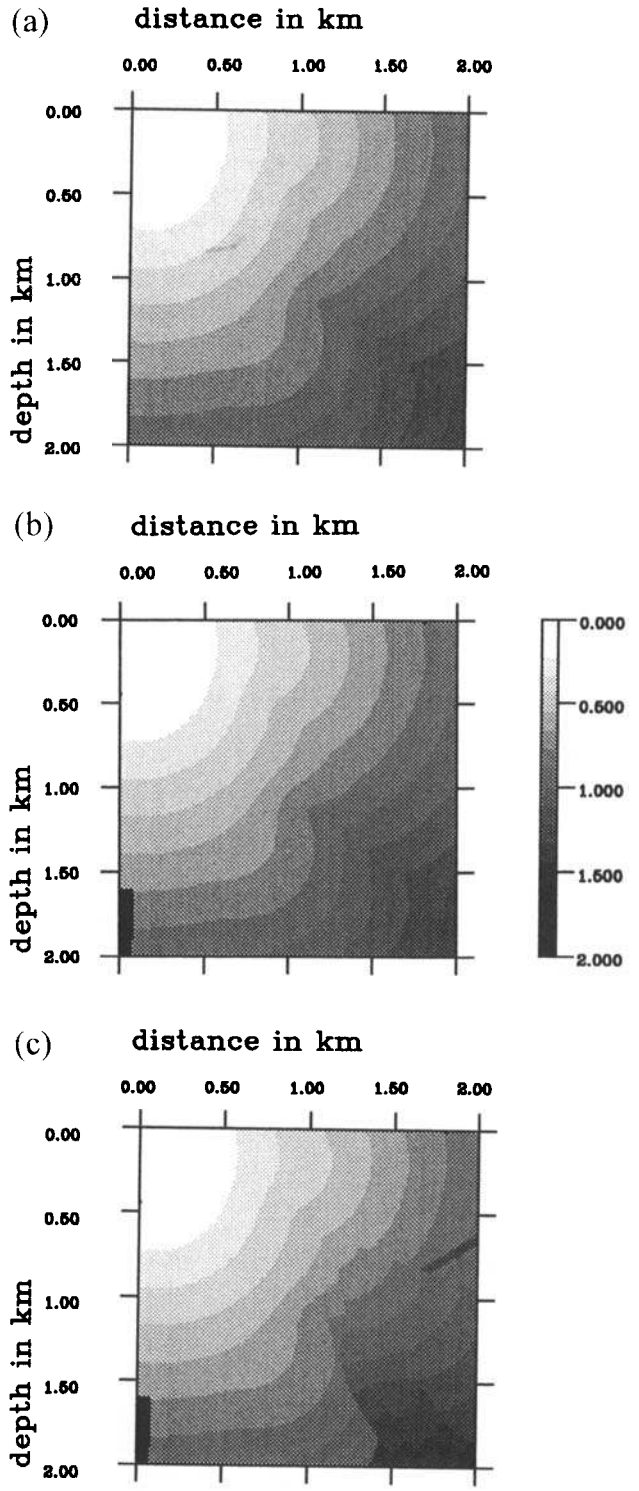

Figure 11. Maps for traveltime obtained for the ray-field sampling presented in Fig. 10: (a) by the algorithm of Podvin & Lecomte (1991); (b) by our algorithm for the first-arrival traveltime; (c) by our algorithm for the strongest-arrival traveltime. The vertical and horizontal steps are 10 m.

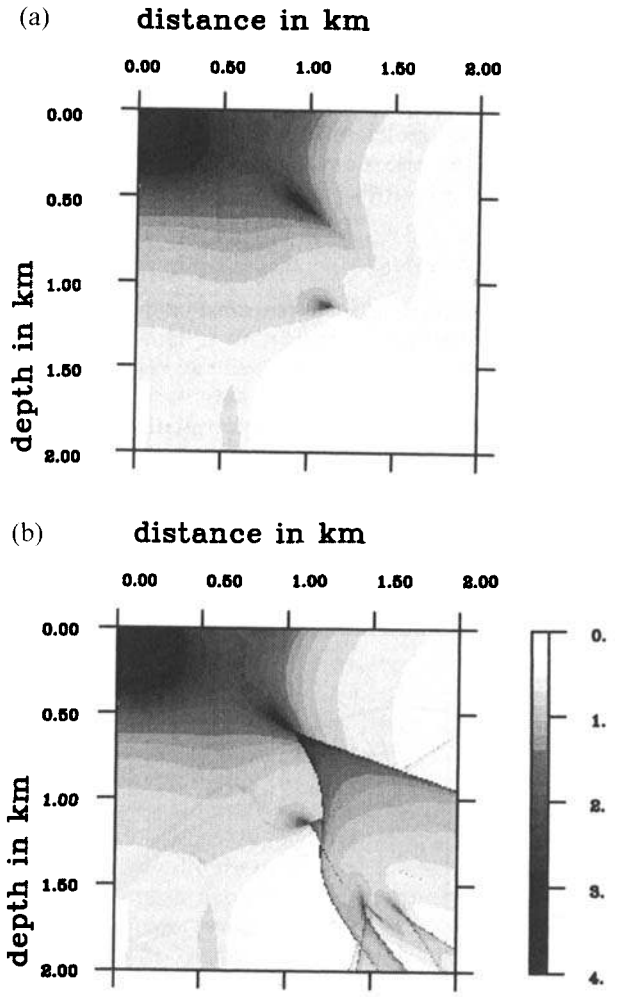

Figure 12. Maps for amplitude obtained for the ray-field sampling presented in Fig. 10: (a) the first-arrival amplitude; (b) the strongest-arrival amplitude. The vertical and horizontal steps are 10 m.

to θ are given by the paraxial parameters. Finally,

$$\begin{cases} \dfrac{\partial^2 \mathbf{x}}{\partial \sigma^2} = \nabla_x \nabla_p H \nabla_p H - \nabla_p \nabla_p H \nabla_x H, \\ \dfrac{\partial^2 \mathbf{p}}{\partial \sigma^2} = -\nabla_x \nabla_x H \nabla_p H + \nabla_p \nabla_x H \nabla_x H, \\ \dfrac{\partial^2 \mathbf{x}}{\partial \sigma \partial \theta} = \dfrac{\partial}{\partial \theta} \nabla_p H, \\ \dfrac{\partial^2 \mathbf{p}}{\partial \sigma \partial \theta} = -\dfrac{\partial}{\partial \theta} \nabla_x H. \end{cases} \tag{23}$$

As we shall see later, the associated error is bounded by the values of our ray-density criterion. The accuracy depends on the constant traveltime step $\Delta\sigma$ chosen initially for sampling Λ and on the values of $dx_{\max}$ and $dp_{\max}$. The precision of interpolation in the θ direction is uniformly bounded, since the ray-density criterion (18) implies that

$$\frac{1}{2}\left|\frac{\partial^2 \mathbf{x}}{\partial \theta^2}\right| \Delta\theta_i^2 < dx_{\max}, \qquad \frac{1}{2}\left|\frac{\partial^2 \mathbf{p}}{\partial \theta_i^2}\right| \Delta\theta_i^2 < dp_{\max}. \tag{24}$$

Unfortunately, paraxial ray theory cannot provide any information about the precision of the interpolated amplitude.

Note that second-order partial derivatives in θ characterize the curvature of the wavefront (σ = constant) in the phase space.

Note also that the precision of linear interpolation of Λ is bounded for an interpolation with respect to the coordinates (θ, σ), but not with respect to (x, z), since the Jacobian matrix $\partial(x, z)/\partial(\theta, \sigma)$ is not invertible at caustics.

7 APPLICATIONS

The ray prolongation scheme presented above assumes a smooth velocity field. This restriction is motivated by the applications in linear inversion, where ray tracing is much faster in a smooth background (Thierry & Lambaré 1995; Ettrich & Gajewski 1995). The implementation of cell ray tracing in velocity models with interfaces has already been developed (Vinje *et al.* 1993a; Pajchel & Moser 1995) and applied in inversion (Moser 1995).

In the most general case, a smooth velocity field can be specified in terms of cardinal cubic B-splines (de Boor 1978). This ensures smoothness up to the second order, which suffices to guarantee the continuity of the paraxial parameters. Integration of eqs (2) and (4) is implemented by a fourth-order Runge–Kutta scheme with a constant step.

The scheme requires further improvements. In particular, sampling in the ray direction should also be controlled and locally adjusted by appropriate cell subdivision. Local reductions of ray density would prevent ray oversampling and improve performance.

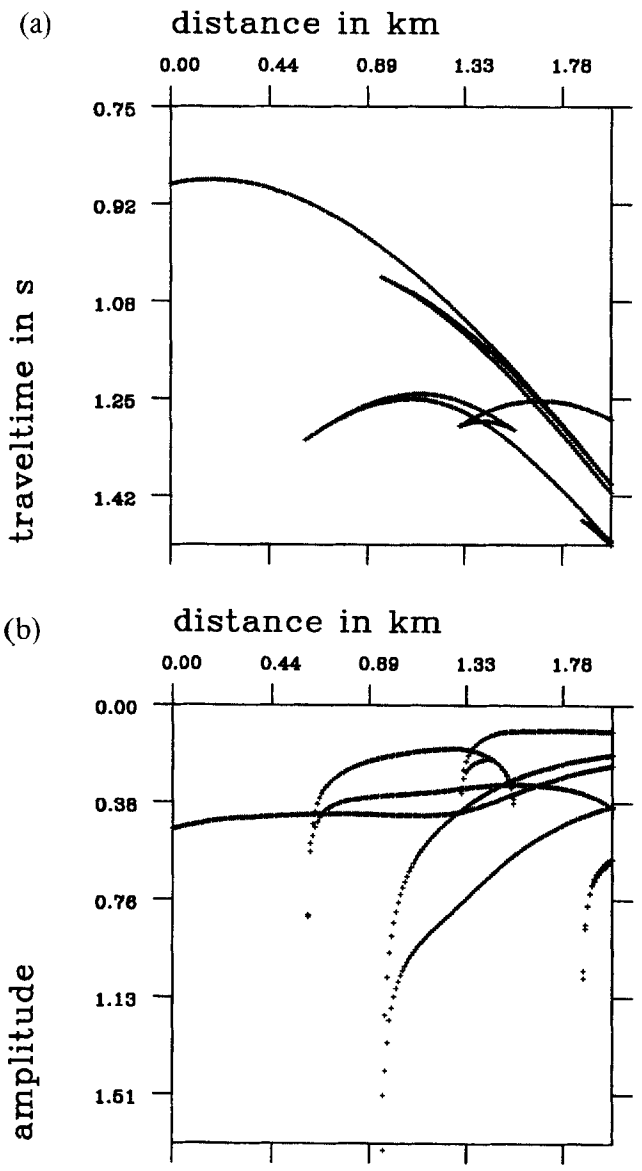

Figure 13. Multivalued traveltimes (a) and amplitudes (b) for a vertical line of receivers at $x = 2000$ m with a vertical step of 10 m obtained by the ray-field sampling presented in Fig. 10. Note numerous triplications and caustics.

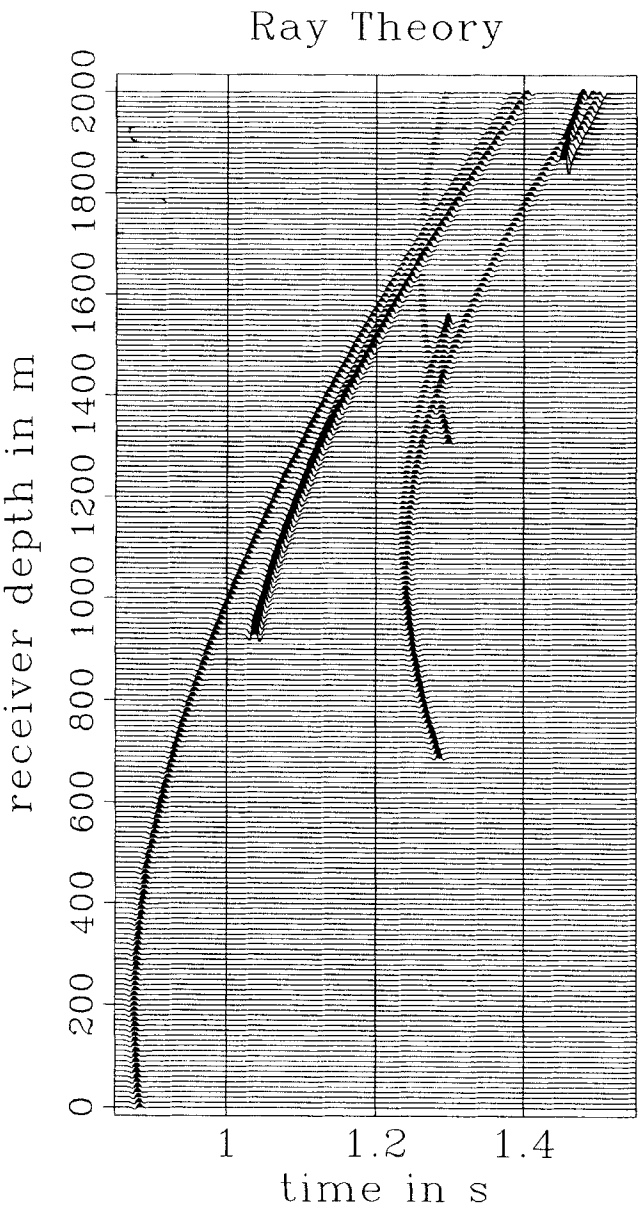

Figure 14. Seismogram obtained from the traveltime and amplitude given in Fig. 12. The phase shift associated with crossing caustics has been taken into account. The source signature is

$$s(t) = \frac{d^2}{dt^2} \exp[-(t/0.005)^2].$$

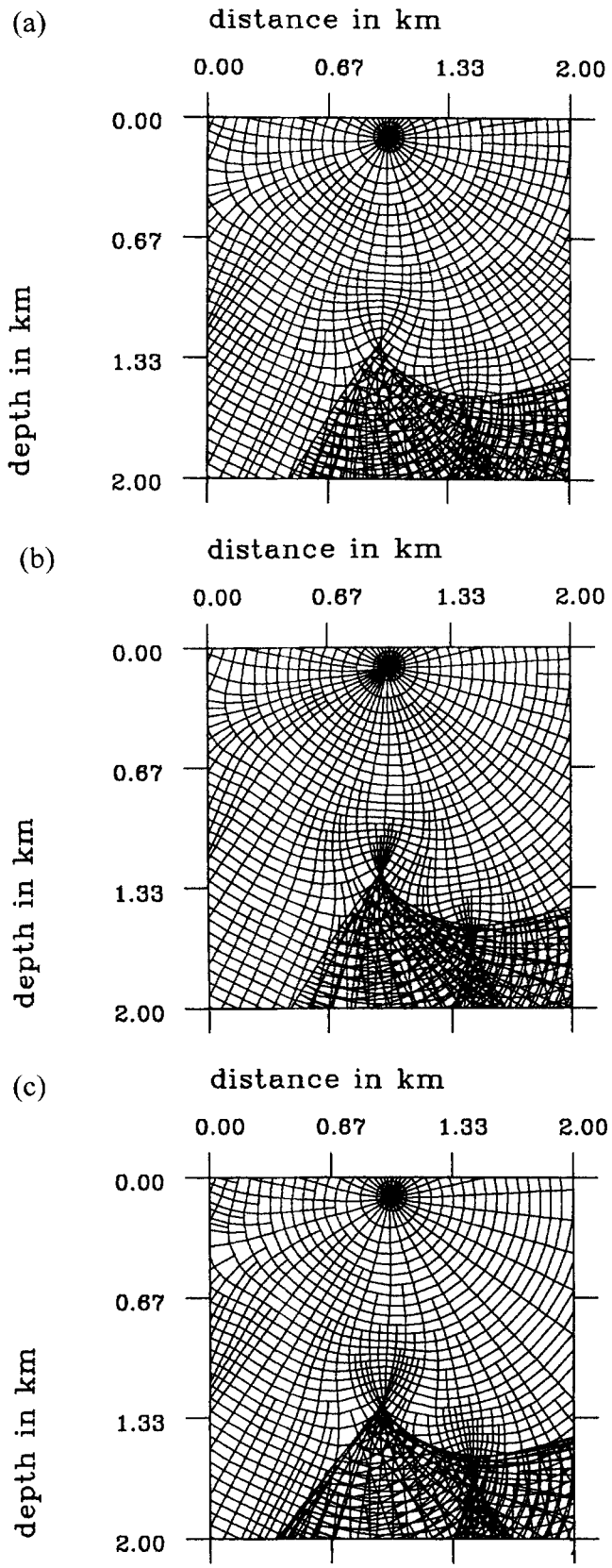

7.1 Choice of the values for dx_{max} and dp_{max}

The tolerances dx_{max} and dp_{max} are related to the desired accuracy of the Lagrangian manifold sampling. We have set dx_{max} equal to the x and z step in the maps, while dp_{max} corresponds to a maximum error in the direction of rays of about 1 to 2 degrees.

7.2 Constant velocity field

In the first place we consider a constant velocity field ($v = 2000$ m s^{-1}). The source point is at $x = 110$ m, $z = 110$ m. Fig. 7 shows the partitioning of the Lagrangian manifold Λ for various 2-D projections of the phase space $[(x, z), (x, p_x), (p_x, z), (p_x, p_z)]$. The traveltime step is 0.03 s, and the ray-density criterion $dx_{max} = 10$ m, $dp_{max} = 10 \times 10^{-6}$ s m^{-1}. Over the (x, z) plane, the rays are straight lines and the wavefronts are circles. The ray field does not exhibit multiple coverage in the configuration space.

7.3 Constant gradient of velocity

In the next example, velocity increases linearly with depth, from 2083 m s^{-1} at $z = 0$ m to 3833 m s^{-1} at $z = 2000$ m. Fig. 8 shows various projections of the Lagrangian manifold Λ. The traveltime step is 0.03 s, and the ray-density criterion is $dx_{max} = 10$ m, $dp_{max} = 10 \times 10^{-6}$ s m^{-1}. The cells are defined by circular rays and wavefronts. This figure can be compared with the previous one. As rays spread apart, new rays are inserted and the cells are subdivided to meet the ray-density criterion. No caustic appears in the configuration space (x, z). One can see a folding of Λ over the plane (x, p_z) at the bottom of the picture. An asymptotic solution in the (x, p_z) domain exhibits a caustic in this region (called a p-caustic). A p-caustic can also be characterized by an infinite (x, p_z)-domain amplitude.

It is a general property of Lagrangian submanifolds that, at every point of a Lagrangian submanifold Λ, at least one of the four projections of Λ on the planes (x, z), (x, p_x), (p_x, z) or (p_x, p_z) is regular (Hanyga 1984). The Fourier transform of the asymptotic solution with respect to the corresponding conjugate pairs of variables (z, p_z), (x, p_x) or both involves a non-vanishing 'ray spreading' Jacobian $\partial(x, p_z)/\partial(\theta, \sigma)$, $\partial(p_x, z)/\partial(\theta, \sigma)$, $\partial(p_x, p_z)/\partial(\theta, \sigma)$. For a caustic in the configuration space one can find a regular asymptotic solution by summing regular asymptotic 'plane' waves corresponding to the fixed value of p_x [in the (p_x, z) domain] or p_z [in the (x, p_z) domain] (Maslov 1972).

7.4 A complex velocity field

Let us now consider a more complex velocity field. The velocity field is the superposition of strong Gaussian heterogeneities

Figure 15. Comparison of ray-density criteria for ray tracing on the complex velocity field presented in Fig. 9. The source is at $x = 1000$ m, $z = 110$ m. The time step is 0.03 s. The ray field is sampled according to: (a) Vinje's criterion; (b) Sun's criterion; (c) our uniform sampling criterion. In order to compare equivalent results in terms of computational cost, we choose the values of the ray-density criteria in such a way as to have the same number of cells (about 2305 in each case).

superposed on a constant background ($v = 2000\ \mathrm{m\ s^{-1}}$) (Fig. 9). 25×25 knot points spaced by 100 m are used for the B-spline representation of the velocity field. The velocity ranges from $1093\ \mathrm{m\ s^{-1}}$ to $3800\ \mathrm{m\ s^{-1}}$. Fig. 10 shows the four projections of the Lagrangian manifold. The source is at $x = 110$ m and $z = 110$ m. The traveltime step is 0.03 s and the ray density is specified by the criterion (18) with $dx_{\max} = 10$ m, $dp_{\max} = 1.0 \times 10^{-5}\ \mathrm{s\ m^{-1}}$. The ray field exhibits many caustics, and projections involve many overlapping cells. The density of rays in the configuration space is increased in the regions of strong curvature of the rays.

Traveltime maps are shown in Fig. 11 for the same parameters as in Fig. 10. The maps are compared with the result obtained for the first-arrival traveltime given by the finite-difference traveltime algorithm of Podvin & Lecomte (1991). The CPU time for the algorithm of Podvin & Lecomte was 0.4 s, as compared with 3.90 s for our ray-tracing code (CPU times are given for a Sparc10 workstation). The latter CPU time breaks down into 1.07 s of ray-field sampling and 2.79 s of linear interpolation of the required parameters (traveltime, amplitude, take-off angle, paraxial ray parameters and the slowness vector). This CPU cost is fairly modest as compared with the CPU cost of the code of Podvin & Lecomte (1991), taking into account that the latter yields only the first-arrival traveltime while our code computes up to nine parameters and gives all the arrivals.

In our tests, the number of cells was 4400 and the number of points in the maps was 201×201 with a step of 10 m. Amplitude maps are shown in Fig. 12. In order to demonstrate the ability of our algorithm to cope with multiple arrivals, Fig. 13 shows the multiple traveltimes and amplitudes for a vertical line of receivers located at $x = 2000$ m. Many caustics can be seen. Infinite amplitudes at caustics are due to the fact that we have applied asymptotic ray theory (ART) to evaluate the field (Fig. 14). These singularities can be eliminated by summation over Λ, as explained in Hanyga *et al.* (1995a). In Fig. 15, comparison of the ray field sampled with the criteria of Vinje *et al.* (1993a) (eq. 15) and Sun (1992) (eq. 16) is shown. In order to compare equivalent results in term of computational cost, we choose the values of the ray-density criteria in such a way as to have the same number of cells (about 2305) in each case. The source is at $x = 1000$ m, $z = 110$ m. The time step is 0.03 s. The complex ray field sampled according to Vinje's criterion (eq. 15) ($dx_{\mathrm{Vinje}} = 100$ m) is shown in Fig. 15(a), while Fig. 15(b) shows the ray field sampled by Sun's criterion (eq. 16) with $dx_{\mathrm{Sun}} = 142$ m, $dp_{\mathrm{Sun}} = 92 \times 10^{-6}\ \mathrm{s\ m^{-1}}$. Fig. 15(c) shows the result of sampling according to criterion (18) with $dx_{\max} = 20$ m, $dp_{\max} = 25 \times 10^{-6}\ \mathrm{s\ m^{-1}}$.

Some attention must be paid to the caustic zones. Vinje's criterion leads to a drastic undersampling in the vicinity of caustics. Sun's criterion brings some improvement at the caustic cusp, but in a neighbourhood of simple caustics the ray field is still drastically undersampled.

We also compared the errors of the ray-field interpolation for the ray fields sampled with the three criteria. As a reference for error estimation, we used a very densely sampled ray field (Fig. 16) obtained with our ray-tracing code with a traveltime

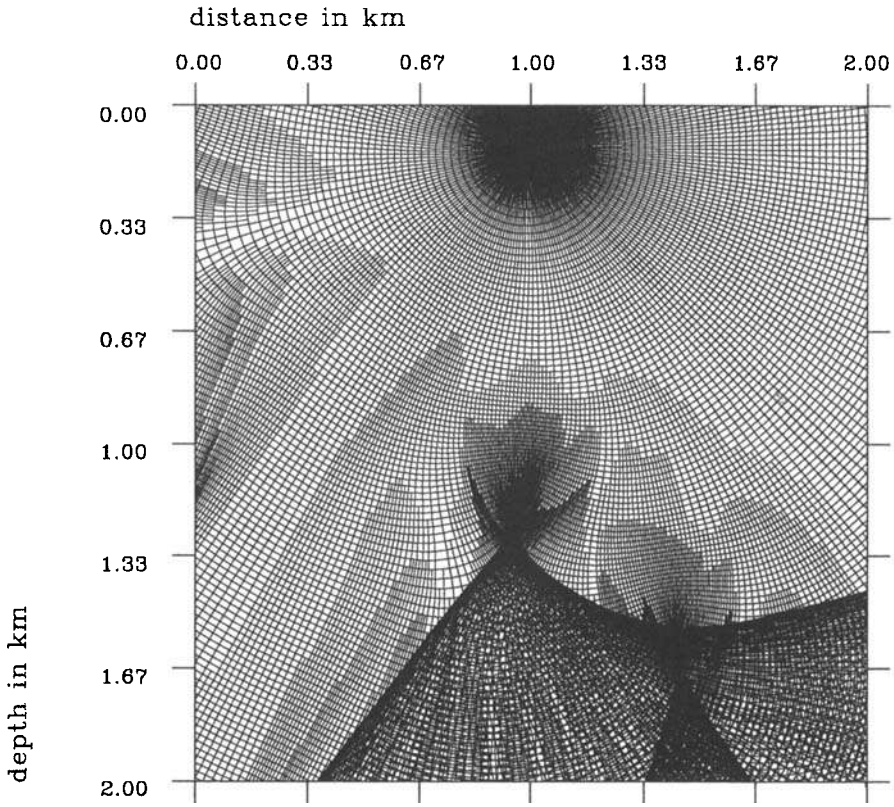

Figure 16. Reference ray-field sampling for testing the accuracy of the ray-field interpolation. The traveltime step is 0.01 s, $dx_{\max} = 1$ m, $dp_{\max} = 10^{-6}\ \mathrm{s\ m^{-1}}$. 37 516 cells were generated.

step of 0.01 s and $dx_{max} = 1.0$ m, $dp_{max} = 10^{-6}$ s m^{-1}. 37 516 cells were generated. Figs 17 and 18 show comparisons between the three criteria, for the errors $|\mathbf{x}_{int} - \mathbf{x}_{ref}|$, and $|\mathbf{p}_{int} - \mathbf{p}_{ref}|$ as functions of the coordinates θ and σ in a region of Λ. Our uniform sampling criterion appears to ensure a better precision, especially in the caustic zones. The error is more uniformly distributed and has smaller extremal values. Sun's criterion gives a little improvement with respect to Vinje's criterion, but still exhibits large errors localized in caustic zones.

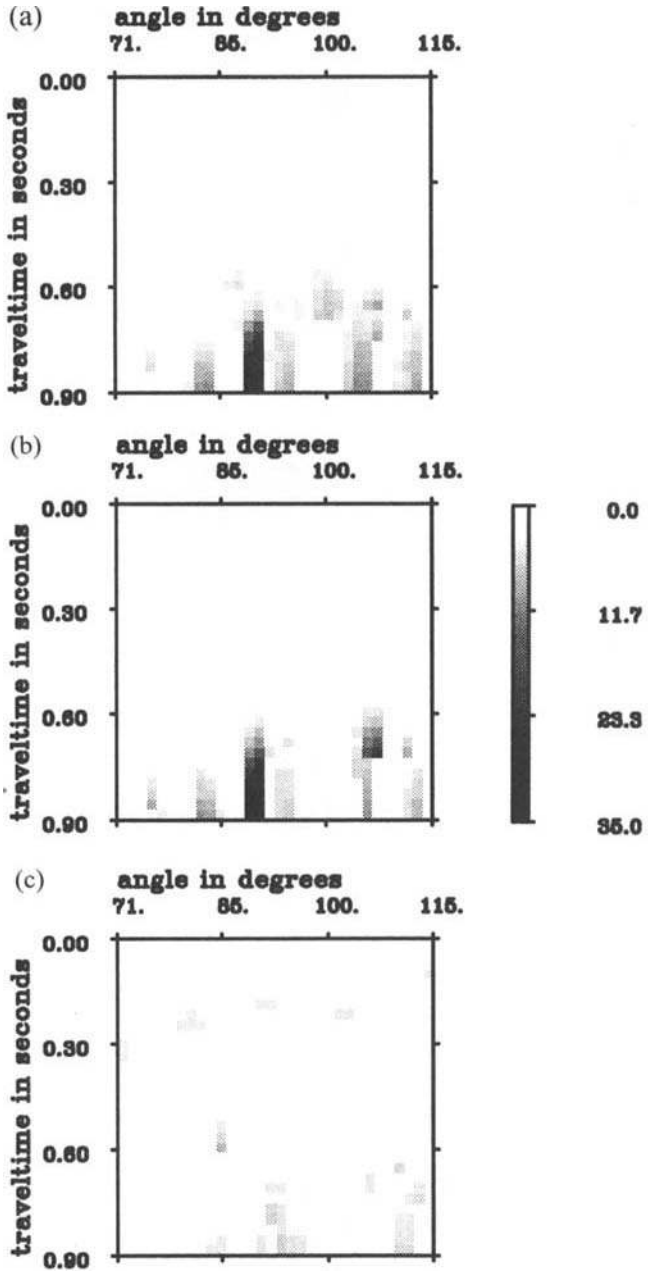

Figure 17. Comparison of the interpolation of the ray field for the various ray-density criteria. This figure presents the error $|\mathbf{x}_{int} - \mathbf{x}_{ref}|$ associated with the linear interpolation of $\mathbf{x}(\theta, \sigma)$ for the ray-field samplings presented in Fig. 15 in respect to the reference sampling shown in Fig. 16. Errors are given in metres for: (a) Vinje's criterion (maximum error 64.9 m); (b) Sun's criterion (maximum error 65.0 m); (c) our uniform sampling criterion (maximum error 8.2 m).

7.5 The Marmousi velocity field

In the last example we applied our algorithm to a smoothed section of the Marmousi model (Fig. 19). The B-spline representation of the velocity field is based on 33 × 34 knot points spaced at 198 m. The source is at $x = 150$ m, $z = 1550$ m. The wavefront spacing is 0.03 s and the ray-density criterion is $dx_{max} = 10$ m, $dp_{max} = 10 \times 10^{-6}$ s m^{-1}. The extreme complexity of the wavefronts can be seen in Fig. 20. Figs 21 and 22 show the maps of traveltimes and amplitudes corresponding respectively to the first arrival and to the most energetic arrival.

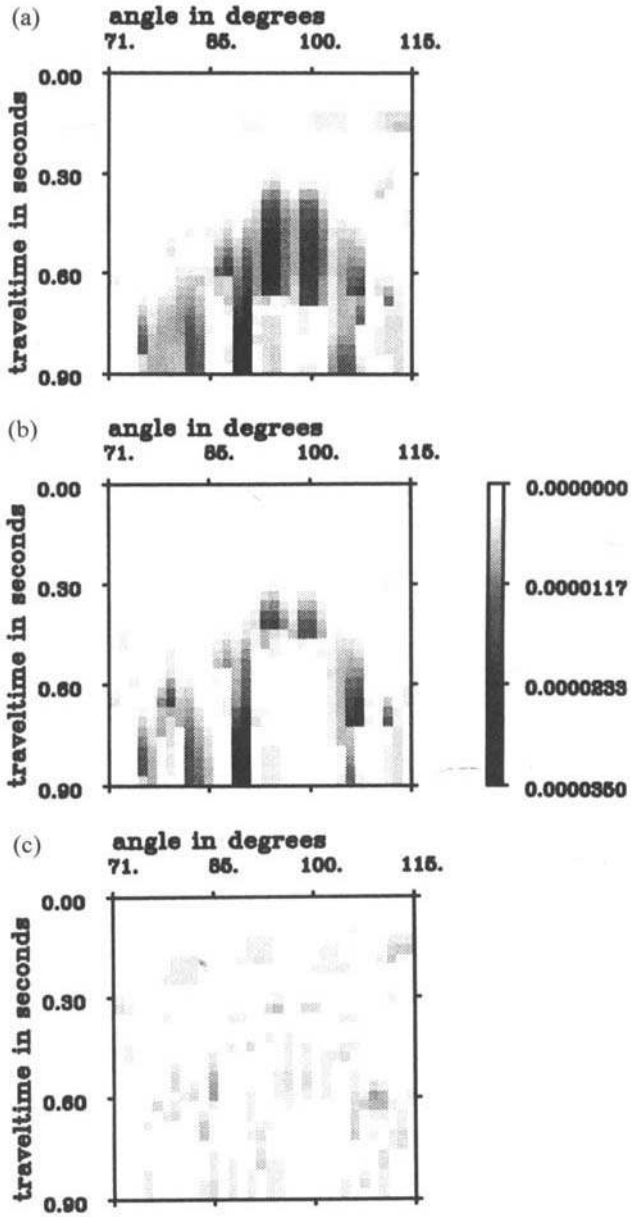

Figure 18. Comparison of the interpolation of the ray field for the various ray-density criteria. This figure presents the error $|\mathbf{p}_{int} - \mathbf{p}_{ref}|$ associated with the linear interpolation of $\mathbf{p}(\Theta, T)$ for the ray field samplings presented in Fig. 15 in respect to the reference sampling shown in Fig. 16. Errors are given in seconds per metres for: (a) Vinje's criterion (maximum error 63.3×10^{-6} s m^{-1}); (b) Sun's criterion (maximum error 63.4×10^{-6} s m^{-1}); (c) our uniform sampling criterion (maximum error 9.9×10^{-6} s m^{-1}).

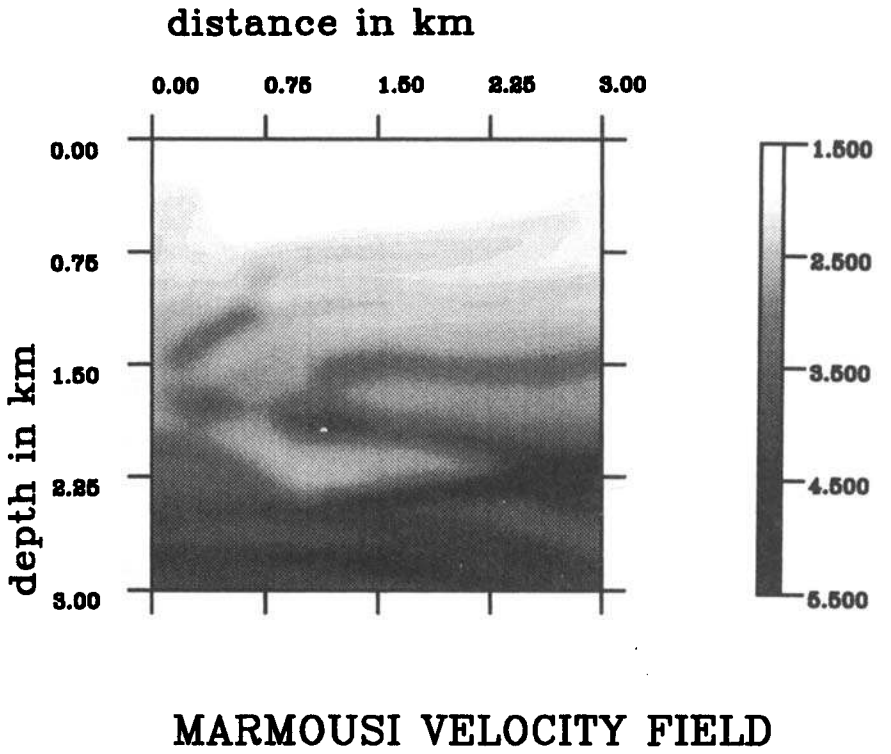

Figure 19. Smoothed section of the Marmousi model. The B-spline representation of the velocity field is based on 33×34 knot points spaced at 198 m.

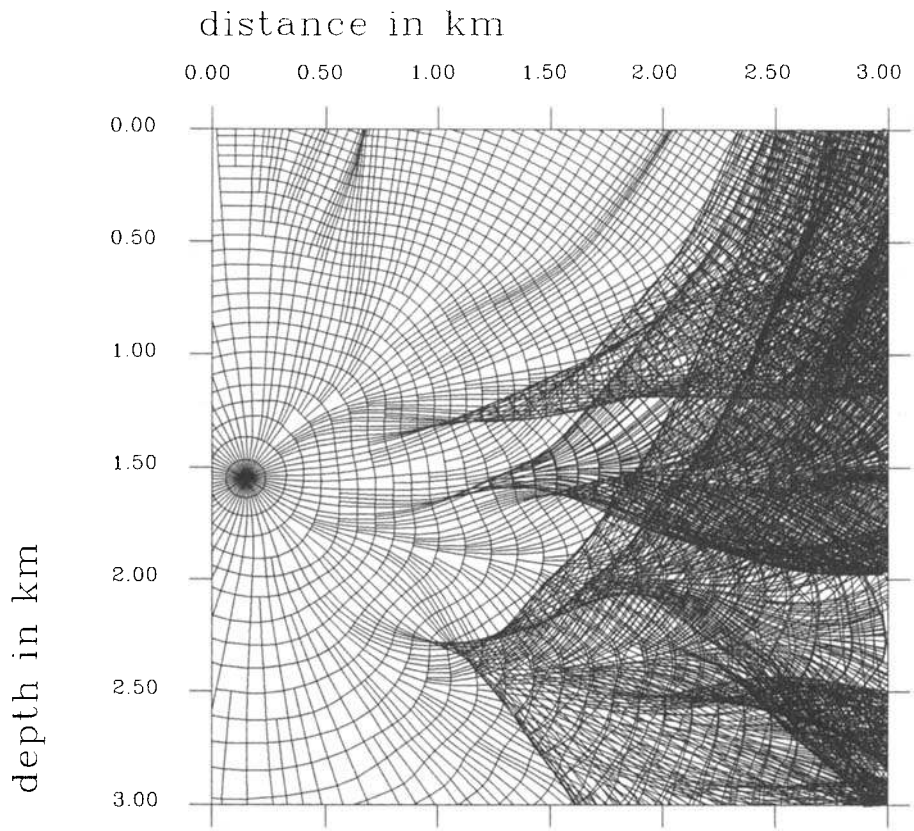

Figure 20. Ray-field sampling in the Marmousi model presented in Fig. 19. The source is at $x = 150$ m, $z = 1550$ m. The wavefront spacing is 0.03 s and the ray-density criterion is $dx_{max} = 10$ m and $dp_{max} = 10 \times 10^{-6}$ s m^{-1}. There are 15 616 cells.

In terms of computational time we have 3.34 s for sampling the ray field (for 15 616 cells) and 9.29 s for interpolating amplitudes and traveltimes (334 × 334 points) on a Sparc10 workstation. The extra computational time for additional interpolation of the take-off angle of the ray, slowness vector and paraxial ray parameters is around 3 s.

8 CONCLUSION

The Hamiltonian approach allows us to deal fairly efficiently with the complexity of the ray field: the singularities appearing in the configuration space are unfolded in the phase space yielding a regular 2-D manifold Λ. Paraxial ray theory allows a control of the sampling of the ray field on Λ. A reliable criterion for uniform sampling of the Lagrangian manifold Λ has been found. It corresponds to a uniform precision of the linear interpolation along selected wavefronts. On the basis of these considerations we have developed a fast and robust algorithm for calculating multivalued maps of traveltimes and amplitudes.

The algorithm is particularly useful for migration and inversion of seismic data. It can naturally be extended to 3-D problems, for which the requirement of fast modelling methods is still more crucial. The 2-D version was developed for testing the concepts that will be applied in three dimension (Lucio *et al.* 1995). Some extensions and applications based on the 2-D version are under development, namely, time-domain Maslov integrals at caustics and caustic cusps (Hanyga, Lambaré & Lucio 1995a) as well as application to 2-D asymptotic inversion (Thierry & Lambaré 1995).

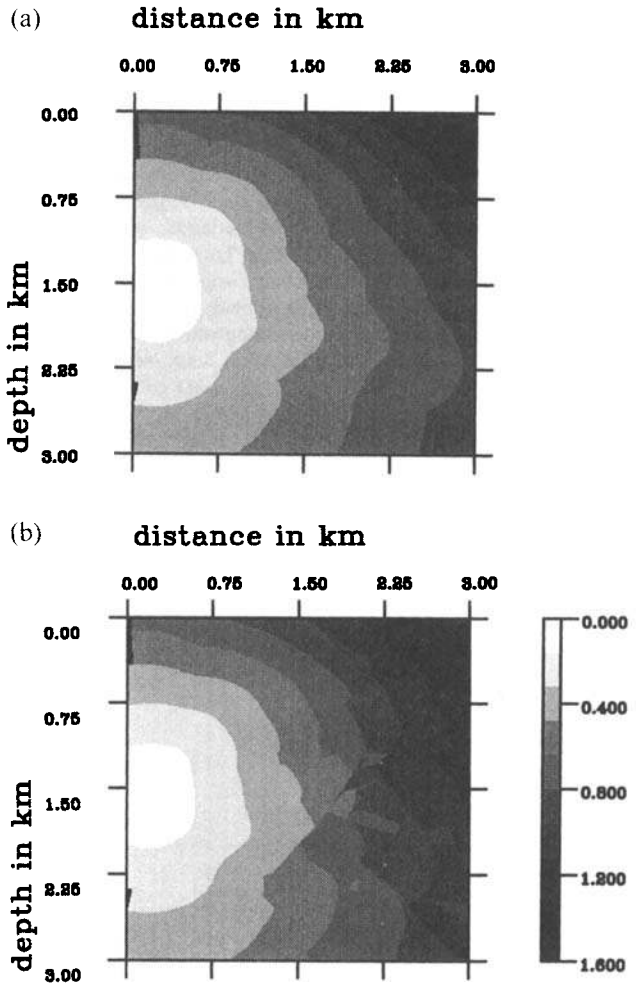

Figure 21. Traveltime maps obtained by the ray-field sampling shown in Fig. 20 on the Marmousi model. There are 334 × 334 points spaced by 10 m in x and z. (a) The first traveltime arrival; (b) the strongest arrival.

ACKNOWLEDGMENTS

This work was partly funded by the European Commission and the Norwegian Research Council in the framework of the JOULE project '3-D Asymptotic Seismic Imaging'. Paulo Lucio was sponsored by a grant from CNPq (Brazil). We are indebted to Patrick Compte from IFP for kindly providing a smoothed Marmousi velocity field, and to Roland Lehoucq (CEA) and Michel Léger for discussions concerning topological

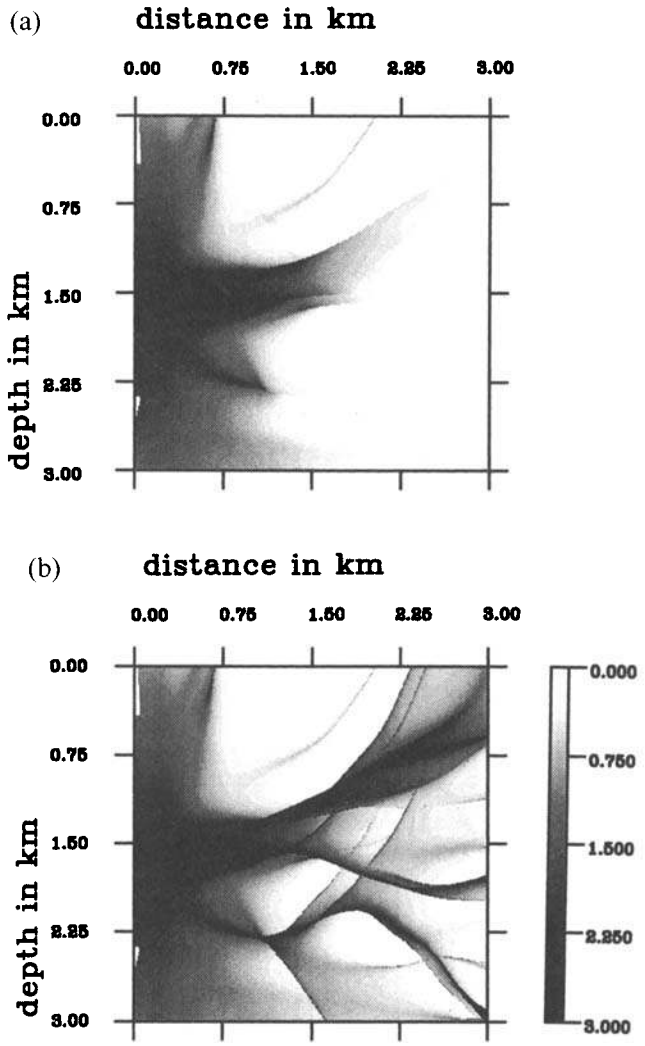

Figure 22. Amplitude maps obtained by the ray-field sampling shown in Fig. 21 on the Marmousi model. There are 334 × 334 points spaced by 10 m in x and z. (a) The first traveltime arrival; (b) the strongest arrival. The difference between the maps agrees with the conclusion of Geoltrain & Brac (1991), concerning the opportunity of using only the minimum traveltime arrival for imaging from the Marmousi data set.

criteria in non-convex space mappings. We are grateful to one of the referees for valuable comments and to Pascal Podvin for discussion and for providing the algorithm for calculating first-arrival traveltime by finite differences.

REFERENCES

Aki, K. & Richards, P., 1980. *Quantitative seismology: Theory and methods,* W.H. Freeman & Co, San Francisco, CA.

Burridge, R., 1976. *Some mathematical topics in seismology,* Courant Institut of Mathematical Sciences, New York University, NY.

Červený, V., 1989. Ray tracing in factorized anisotropic inhomogeneous media, *Geophys. J. Int.,* **99,** 91–100.

Chapman, C.H., 1985. Ray theory and its extensions: WKBJ and Maslov seismogram, *J. Geophys.,* **58,** 27–43.

de Boor, C., 1978. *A practical guide to splines,* Springer-Verlag, Berlin, Germany.

Ettrich, N. & Gajewski, D., 1995. Efficient prestack Kirchhoff migration using wavefront construction, extended abstract 57th EAEG Meeting, Glasgow, A023, EAEG, Zeist, Netherlands.

Farin, G., 1993. *Curves and surfaces for computer aided geometric design: a practical guide,* 3rd edn, Academic Press, San Diego, CA.

Farra, V. & Madariaga, R., Seismic waveform modeling in heterogeneous media by ray perturbation theory, *J. geophys. Res.,* **92,** 2697–2712.

Forgues, E., Lambaré, G., de Beukelaar, P., Coppens, F. & Richard, V., 1994. An application of Ray + Born inversion on real data, in *SEG Ann. Meetg, Expanded Abstracts,* pp. 1004–1007, Los Angeles, SEG, Tulsa, OK.

Geoltrain, S. & Brac, J., 1991. Can we image complex structures with finite-difference travel times?, in *61th SEG Ann. Meetg, Expanded Abstracts,* pp. 1110–1113, SEG, Tulsa, OK.

Goldstein, H., 1980. *Classical Mechanics,* (1st edn 1950) Addison-Wesley, Reading, MA.

Guillemin, V. & Sternberg, S., 1977. *Geometric Asymptotics,* American Mathematical Society, Providence, RI.

Hanyga, A., 1984. Dynamic ray tracing on Lagrangian manifolds, *Geophys. J. R. astr. Soc.,* **79,** 51–63.

Hanyga, A. & Helle, H.B., 1995. Synthetic seismograms from generalized ray tracing, *Geophys. Prospect.,* **43,** 51–76.

Hanyga, A., Lenartowicz, E. & Pajchel, J., 1985. *Seismic Waves in the Earth,* Elsevier, Amsterdam.

Hanyga, A., Lambaré, G. & Lucio, P.S., 1995a. Asymptotic Green's functions by Maslov summation, *SEG Ann. Meetg, Extended Abstracts,* pp. 1297–1300, SEG, Tulsa, OK.

Hanyga, A., Thierry, P., Lambaré, G. & Lucio, P., 1995b. 2D and 3D asymptotic Green's functions for linear inversion, in *Mathematical Methods in Geophysical Imaging III,* pp. 123–137, ed. Hassanzadeh, S., *Proc. SPIE,* **2571,** SPIE, Bellingham, WA.

Lambaré, G., Virieux, J., Madariaga, R. & Jin, S., 1992. Iterative asymptotic inversion in the acoustic approximation, *Geophysics,* **57,** 1138–1154.

Lucio, P.S., Lambaré, G. & Hanyga, A., 1995. 3D multivalued travel time and amplitude map, in *57th EAEG Meetg, Expanded Abstracts,* p. 147, EAEG, Zeist, Netherlands.

Maslov, V.P., 1972. *Théorie des perturbations et méthodes asymptotiques,* Dunod et Gauthier-Villars, Paris.

Moser, T.J., 1995. Inversion in a nonsmooth background, *57th EAEG Meetg, Expanded Abstracts,* E036, EAEG, Zeist, Netherlands.

Pajchel, J., Moser, T.J., 1995. Recurcive cell raytracing, *57th EAEG Meetg, Expanded Abstracts,* P092, EAEG, Zeist, Netherlands.

Pham, F., 1992. *Géométrie et calcul différentiel sur les variétés: Cours, études et exercices pour la maîtrise de mathématiques,* InterÉditions, Paris.

Podvin, P. & Lecomte, I., 1991. Finite difference computation of travel times in very contrasted velocity models: a massively parallel approach and its associated tools, *Geophys. J. Int.,* **105,** 271–284.

Sun, Y., 1992. Computation of 2D multiple arrival travel time fields by an interpolative shooting method, in *62th SEG Ann. Meetg, Expanded Abstracts,* pp. 1320–1323, SEG, Tulsa, OK.

Thierry, P. & Lambaré, G., 1995. 2.5D true amplitude migration on a workstation, *SEG Ann. Meetg, Extended Abstracts,* pp. 156–159, SEG, Tulsa, OK.

Vidale, J., 1988. Finite-difference calculation of travel time, *Bull. seism. Soc. Am.,* **78,** 2062–2076.

Vinje, V., Iversen, E. & Gjøystdal, H., 1992. Traveltime and amplitude estimation using wavefront construction, in *EAEG Ann. Meetg, Abstract,* pp. 504–505, EAEG, Zeist, Netherlands.

Vinje, V., Iversen, E. & Gjøystdal, H., 1993a. Traveltime and amplitude estimation using wavefront construction, *Geophysics,* **58,** 1157–1166.

Vinje, V., Iversen, E., Gjøystdal, H. & Åstebøl, K. 1993b. Estimation of multivalued arrivals in 3D models using wavefront construction, *EAEG Ann. Meetg. Abstract,* B019, EAEG, Zeist, Netherlands.

Virieux, J. & Farra, V., 1991. Ray tracing in 3D complex isotropic media: an analysis of the problem, *Geophysics,* **56,** 2057–2069.

Weinstein, A., 1979. *Lectures on symplectic manifold,* AMS, Providence, RI.